Switching current measurements of large area Josephson tunnel junctions

A. Wallraff,[a] A. Lukashenko, C. Coqui, A. Kemp, T. Duty,[b] and A. V. Ustinov
Physikalisches Institut III, Universität Erlangen–Nürnberg, D-91058 Erlangen, Germany

(Received 6 March 2003; accepted 21 April 2003)

We have developed a scheme for high resolution measurements of the switching current distribution of a current-biased Josephson tunnel junction using a timing technique. In the measurement setup digital control and read-out electronics are galvanically isolated from the analog sample bias electronics by an optical fiber link. We have successfully used this technique to investigate thermal activation and macroscopic quantum tunneling of the phase in a high-quality $5\times5\ \mu\mathrm{m}^2$ Nb–Al/AlO_x–Nb Josephson tunnel junction with a critical current of $I_c\approx325\ \mu$A. At temperatures above the cross over temperature of $T^\star\approx280$ mK the escape is dominated by thermal activation. Due to the high quality factor of the junction ($Q\approx95$), the escape temperature is noticeably affected by the thermal prefactor. At temperatures below $T^\star$, the value of which agrees well with the theoretical predictions, the escape of the phase by quantum mechanical tunneling is observed. The presented technique can be employed to characterize current-biased Josephson tunnel junctions for applications in quantum information processing. © *2003 American Institute of Physics.*
[DOI: 10.1063/1.1588752]

I. INTRODUCTION

The current-biased Josephson tunnel junction is an ideal system with which to study both thermal activation and quantum tunneling in a controllable experimental environment.[1] The dynamics of such a junction are equivalent to those of a particle in a tilted washboard potential.[2,3] The process of particle escape from a metastable state in this system can be characterized by analyzing the transition of the particle from a state in which it is localized in a potential well to a state in which it runs down the potential. This corresponds to a transition of the Josephson junction from a superconducting zero-voltage state to a finite voltage state in the presence of applied bias current. At high temperatures escape is dominated by thermal activation across the barrier,[4,5] at low temperatures it is determined by quantum tunneling through the barrier.[6] The rate at which the particle escapes from the well depends on details of the shape of the potential, dissipation in the system, and the temperature of the thermal bath to which the system is coupled.

Thermal activation (TA) in a current-biased Josephson junction has been studied both theoretically and experimentally for large damping,[7,8] intermediate to low damping,[9–11] and extremely low damping.[11,12] At low temperatures the quantum mechanical properties of Josephson junctions have been investigated in relation to macroscopic quantum tunneling (MQT),[13–15] energy level quantization (ELQ),[12,16,17] and macroscopic quantum coherence (MQC).[18–20] Recently, the quantum mechanical properties of Josephson junction systems have gained renewed interest in view of their possible application to solid state quantum information processing.[21–25] The prospect of superconducting devices that contain Josephson junctions for use as carriers of quantum information has been strengthened by recent encouraging experimental results.[19,20,26–31]

In this article we present a measurement technique that is implemented for the characterization of quantum properties of current-biased Josephson tunnel junctions which can be used as phase qubits.[19,20] The measurement scheme is based on a high resolution measurement of the junction's switching current[9] using a timing technique. The measurement setup was tested by performing measurements of both thermal activation and quantum tunneling of the phase in a Josephson junction.

In Sec. II, the Stewart–McCumber model that describes the dynamics of the phase in a Josephson junction is briefly reviewed in relation to thermal activation and quantum tunneling of the phase. The measurement technique and the setup implemented are described in Sec. III. The switching current distributions acquired to test the setup are presented in Sec. IV. In Sec. V, data in the thermal regime are analyzed, the crossover temperature to the quantum regime is determined, and the measured switching current distributions are compared to quantum predictions. Finally, the results are discussed in Sec. VI.

II. MODEL

In the Stewart–McCumber model,[2,3] the dynamics of a current-biased Josephson tunnel junction are described by an equation of motion for the phase difference, ϕ,

$$C\left(\frac{\Phi_0}{2\pi}\right)^2\ddot{\phi}+\frac{1}{R}\left(\frac{\Phi_0}{2\pi}\right)^2\dot{\phi}+I_c\frac{\Phi_0}{2\pi}\sin(\phi)-I\frac{\Phi_0}{2\pi}=0, \quad (1)$$

where Φ_0 is the magnetic flux quantum. In Eq. (1), C is the effective shunt capacitance and R is the effective shunt resistance of the junction embedded in the bias circuitry;[1] see Fig. 1(a). I_c is the fluctuation free critical current of the

[a]Current address: Dept. of Applied Physics, Yale University, New Haven, CT 06511-8284; electronic mail: andreas.wallraff@yale.edu
[b]Previous address: D-Wave Systems Inc. 1985 West Broadway, Vancouver, BC V6J 4Y3, Canada; current address: Dept. of Microelectronics and Nanoscience, MC2, Chalmers University of Technology and Göteborg University, S-412 96 Gothenburg, Sweden.

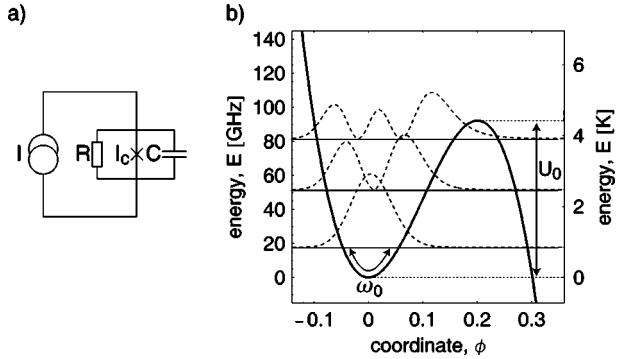

FIG. 1. (a) Resistive, capacitively shunted junction (RCSJ) model. (b) U vs ϕ calculated for a junction with the parameters used in the experiments and bias of $\gamma=0.995$. Barrier height U_0 and oscillation frequency ω_0 are indicated. Numerically calculated energy levels and the square of wave functions are shown.

junction and I is the externally applied bias current. The equation of motion, Eq. (1), is equivalent to damped motion of a particle of mass $m=C(\Phi_0/2\pi)^2$ in an external potential $U(\phi)$ along the generalized coordinate ϕ,

$$m\ddot{\phi}+m\frac{1}{RC}\dot{\phi}+\frac{\partial U(\phi)}{\partial\phi}=0. \tag{2}$$

In Eq. (2) the damping coefficient is $1/RC$ and the potential is given by

$$U(\phi)=-E_J(\gamma\phi+\cos\phi), \tag{3}$$

where $E_J=\Phi_0 I_c/2\pi$ is the Josephson coupling energy and $\gamma=I/I_c$ is the normalized bias current. $U(\phi)$ is a cosinusoidal potential, Eq. (3), with amplitude proportional to E_J, which is tilted proportionally to the bias current γ applied. Because of these properties $U(\phi)$ is often called a washboard potential.

In the absence of thermal and quantum fluctuations and for bias currents $\gamma<1$, the junction is in the zero-voltage state, which corresponds to the particle being localized in one of the potential wells [see Fig. 1(b)]. At finite temperatures $T>0$, the particle may escape from the well at bias currents $\gamma<1$ by thermally activated processes[8–10,32–34] and also by quantum tunneling through the barrier.[12–15,35] The rate at which both processes occur depends on the barrier height

$$U_0=2E_J[\sqrt{1-\gamma^2}-\gamma\arccos(\gamma)], \tag{4}$$

the oscillation frequency of the particle at the bottom of the well,

$$\omega_0=\sqrt{\frac{\partial^2 U/\partial\phi^2}{m}}=\omega_p(1-\gamma^2)^{1/4}, \tag{5}$$

and damping in the junction. Here $\omega_p=\sqrt{2\pi I_c/\Phi_0 C}$ is the plasma frequency. For $\gamma\to1$, Eq. (4) can be approximated as

$$U_0\approx E_J\frac{4\sqrt{2}}{3}(1-\gamma)^{3/2}. \tag{6}$$

At high temperatures the escape of the particle from the well is dominated by thermally activated processes, which occur at a bias-current dependent rate of[4,5]

$$\Gamma_t=a_t\frac{\omega_0}{2\pi}\exp\left(-\frac{U_0}{k_BT}\right), \tag{7}$$

where a_t is a temperature and damping dependent thermal prefactor.

As the temperature T is lowered, thermal activation is exponentially suppressed. At temperatures below the so-called crossover temperature $T^\star=\hbar\omega_0/2\pi k_B$ the quantum tunneling rate of the particle through the barrier exceeds the thermal activation rate.[36] The tunneling rate of the phase is calculated within the Wentzel–Kramers–Brillouin (WKB) approximation for a particle of mass m tunneling through the potential barrier described by U. The effect of damping with the characteristic coefficient $a=1/(2RC\omega_0)=1/(2Q)$, where $Q=\omega_0 RC$ is the quality factor of the junction, is considered in terms of coupling to a bath of harmonic oscillators.[6,37,38] The tunneling rate is then given by

$$\Gamma_q=A\exp(-B), \tag{8}$$

with

$$A=\sqrt{60}\omega_0\left(\frac{B}{2\pi}\right)^{1/2}[1+O(a)], \tag{9}$$

$$B=\frac{36U_0}{5\hbar\omega_0}[1+1.74a+O(a^2)]. \tag{10}$$

As in Eq. (7), the values of Γ_q, U_0, and ω_0 depend on I.

At low temperatures and small damping the energy of the small oscillations of the phase at the bottom of the well is quantized; see Fig. 1(b). Quantization of the energy level has been observed experimentally both below[12,17] and above $T^\star$.[16,39]

III. MEASUREMENT TECHNIQUE AND SETUP

The escape of the phase in a Josephson tunnel junction is experimentally investigated by measuring the statistics of switching of the junction from its zero-voltage state to a finite voltage state. There are two different well established methods that one can use to perform the measurement. In the first method, a bias current applied to the junction is ramped up at a constant rate $\dot{I}$ and the current I at which the junction switches from its zero-voltage to a finite voltage state is recorded.[9] The probability distribution $P(I)$ of such switching currents is found by accumulating a large number of measurements of I and generating a histogram. Using the $P(I)$ distribution, the bias current dependent escape rate $\Gamma(I)$ can be reconstructed as[9]

$$\Gamma(I)=\frac{\dot{I}}{\Delta I}\ln\frac{\int_I^\infty P(I')dI'}{\int_{I+\Delta I}^\infty P(I')dI'}. \tag{11}$$

The results can be compared with the theoretical predictions of Eqs. (7) and (8). In the second method, a fixed bias current $I<I_c$ is applied to the junction at an initial time t and the time delay Δt until a voltage across the junction appears is determined.[18,40] From statistical distribution of the times measured Δt, the lifetime $\tau(I)$ of the junction in the zero-voltage state may be determined. The inverse of the lifetime $\tau(I)$ corresponds to the escape rate $\Gamma(I)$.

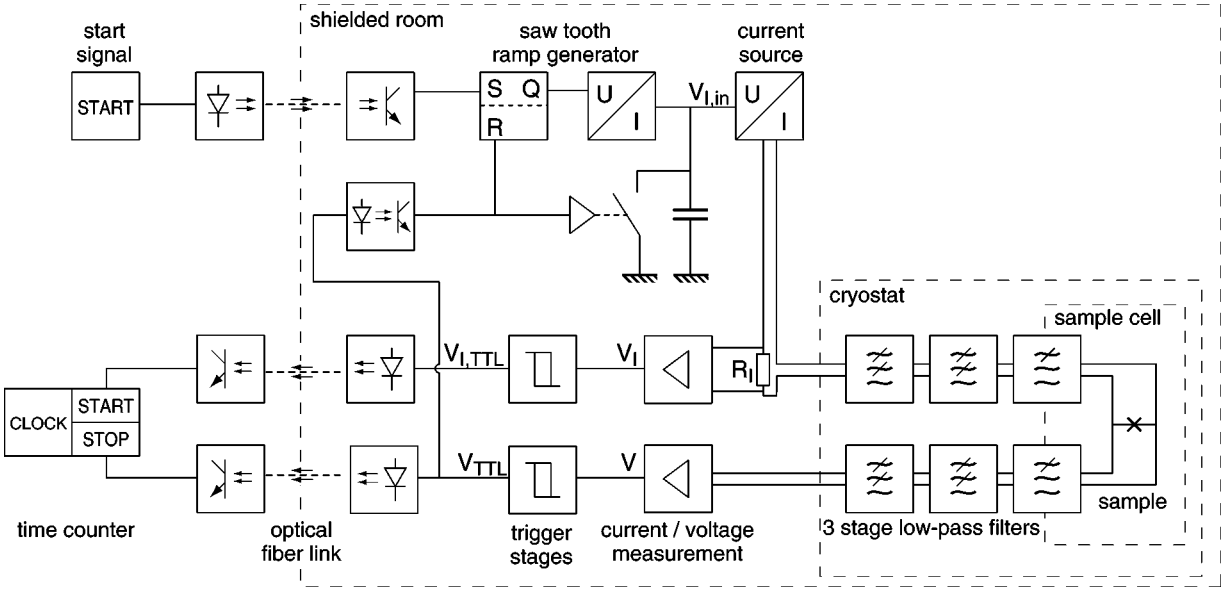

FIG. 2. Schematic of the measurement setup. (A detailed explanation is found in the text.)

We have developed an experimental setup to investigate the transition of a Josephson tunnel junction from its zero-voltage to a finite voltage state using a high resolution measurement of its switching current distribution. In our setup the switching current is determined by measuring the time delay between zero crossing of a linear bias current ramp applied to the sample and switching of the junction to the finite voltage state. The measurement is performed with high precision using a universal time interval counter based on a 20 GHz time base. The timing approach to the current measurement allows us to isolate the analog sample biasing electronics from the digital control electronics using an optical fiber link, which dramatically reduces electromagnetic interference and noise in the setup.

Here in Sec. III A the components of the setup are discussed in detail starting with the sample cell mounted at the cold finger of the dilution refrigerator, the cold and warm filters in the dc-bias lines, the room temperature analog electronics, the optical fiber link, and finally digital control and the data acquisition electronics. A schematic of the layout of the setup is shown in Fig. 2. We also discuss the current resolution achievable with this technique.

A. Sample cell and wiring

The sample, typically fabricated on a $5\times5\,\mathrm{mm}^2$ oxidized Si chip, is mounted in a hermetic copper cell that shields it from electromagnetic radiation in the environment. The sample cell is thermally anchored on the cold finger of a dilution refrigerator.

To current bias the junction and measure the voltage across it, four wires are fed through microwave filters into the sample cell. In the cell the wires are thermally anchored and connected via wire bonds to the junction. Each microwave filter section is made from a commercially available[41] 1 m long, 0.5 mm diam lossy stainless steel coaxial line with a 50 Ω/m Ni/Cr (80%/20%) inner conductor. This type of filter, also called a thermocoax filter,[42] has attenuation of more than 50 dB/m at frequencies above 1 GHz and is directly soldered into the wall of the sample cell. Alternatively, we have used copper powder microwave filters[12] consisting of a few meters of resistive wire coiled up in a 10 cm long copper tube filled with 10 μm grain-size copper powder and mounted in the wall of the cell. To minimize heating of the filters at large bias currents, the total dc resistance of the filter may be adjusted by choosing appropriate wire cross sections or materials. We have designed these filters to have attenuation of more than 50 dB per section above 1 GHz. All additional wires required for heaters, temperature sensors, coils, etc. were fed into the cell through microwave filters of either type. An alternative type of cryogenic microwave filter, not tested in our setup, is based on a microfabricated distributed RLC circuit.[43]

From the sample cell the bias leads are passed to the 1 K stage of the cryostat in a tightly twisted loom of superconducting wires, which is thermally anchored at a number of points. All wires are fed through a low pass RC-filter stage, which is thermally anchored at the 1 K pot and realized with surface mounted components. The RC filters have a 3 dB cutoff frequency of approximately 50 kHz.

The wiring is further fed to the top of the cryostat in a loom of twisted copper pairs in a shield separated from the sensor and control wiring of the cryostat. At room temperature all wires are passed through low pass π-type feedthrough filters with cutoff frequency of about 10 MHz. After the last filtering stage the wires are separated into shielded pairs which are connected to the analog battery-powered bias electronics.

B. Analog electronics, data acquisition, and digital control

The switching current measurement is performed by ramping up the bias current at fixed rate $\dot{I}$ starting from a small negative bias; see Fig. 3(a). Zero crossing of the current is detected using a trigger circuit set to threshold current I_{th} which produces a start pulse for the time measurement at

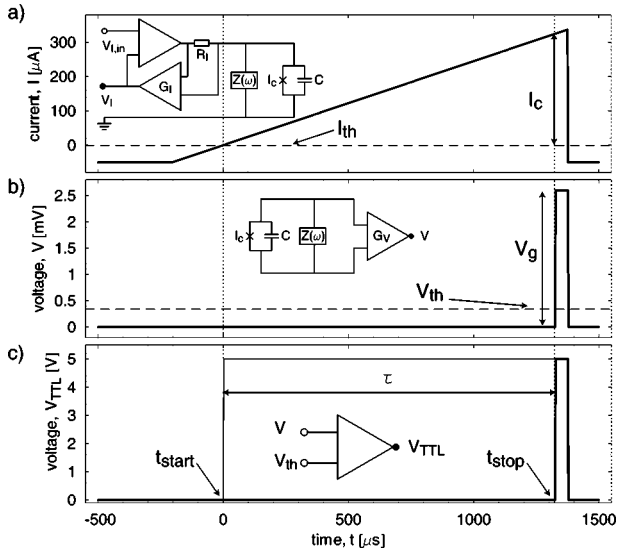

FIG. 3. Principle behind measurement: (a) Bias current vs time. The critical current I_c and current trigger threshold $I_{\rm th}$ are indicated. (b) Measured voltage vs time. The gap voltage V_g and the voltage trigger threshold $V_{\rm th}$ are indicated. (c) Trigger signals $V_{\rm TTL}$ and $V_{I,\rm TTL}$ vs time. The rising edges of both signals are indicated by $t_{\rm start}$ and $t_{\rm stop}$, respectively. Respective simplified circuit diagrams are shown in the insets.

$t=t_{\rm start}$; Fig. 3(c). The drop in voltage across the junction is detected by a second trigger circuit set to a threshold voltage of $V_{\rm th}$; Fig. 3(b), which generates a stop pulse at $t=t_{\rm stop}$. The switching current I is then determined to be $I=\dot{I}\tau$, where $\tau=t_{\rm stop}-t_{\rm start}$ is the time measured, see Fig. 3(c). After the switching current has been detected the bias current is reset to its initial value in order to reduce heating of the sample to a minimum.

The sample is current biased using a voltage controlled current source with selectable output current ranges. The source current I is proportional to the input voltage $V_{I,\rm in}$ in the range of -10 to 10 V. The control voltage $V_{I,\rm in}$ is a sawtooth wave form with an adjustable voltage ramp rate generated by charging a capacitor with constant current. The sawtooth signal is started by a digital trigger signal at the set input (S). The voltage ramp is stopped by a digital trigger signal at the reset input (R); see Fig. 2.

The current flowing through the sample is monitored by measuring the drop in voltage V_I across the biasing resistor R_I using an instrumentation amplifier. The spectral density of the voltage noise S_V^I in V_I has been determined to be less than 20 nV/$\sqrt{\rm Hz}$. In the 0–100 kHz band this amounts to a root mean square (rms) value of $\delta V_{I,\rm rms}\approx 6\ \mu$V.

The drop in voltage V across the junction is measured using a fast field effect transistor (FET) instrumentation amplifier. The spectral density of the voltage noise of the amplifier was measured with the sample biased in the zero-voltage state and connected to the input of the amplifier operated at a gain of $G_V=10^3$. The inferred input noise level of $S_V\approx 13$ nV/$\sqrt{\rm Hz}$ at 10 kHz is close to the specifications of the amplifier. At $G_V=10^3$ the noise level rolls off at 50 kHz, in agreement with the specified bandwidth of the amplifier. The inferred rms input voltage noise in the full band is $\delta V_{\rm rms}\approx 6\ \mu$V.

Both voltages V_I and V are fed to two independent Schmidt triggers with adjustable threshold voltage and hysteresis. The current trigger is calibrated to generate a transistor transistor logic (TTL) pulse $V_{I,\rm TTL}$ upon zero-crossing of the bias current, i.e., at the threshold current $I_{\rm th}=0$ corresponding to the threshold voltage $V_{I,\rm th}=R_I I_{\rm th}$. The voltage trigger generates a TTL pulse $V_{\rm TTL}$ at the voltage threshold $V_{\rm th}\approx 400\ \mu$V when the junction switches from the zero-voltage to a finite voltage state. The integrated input voltage noise of the comparators used in the trigger circuits is $\delta V_{\rm trig,rms}\approx 20\ \mu$V. The trigger hysteresis is adjusted to avoid noise voltage induced triggering. The voltage trigger signal $V_{\rm TTL}$ is also used to stop the current ramp. To avoid a ground loop the reset input of the sawtooth generator is galvanically decoupled using an optical isolator.

All analog electronics components described above have been specifically designed and implemented for these measurements. The supply voltage is delivered by lead batteries. Ground loops are avoided by careful design of the wiring and by optical isolation. All electronics are grounded at a single grounding point on the top of the cryostat. The cryostat and the analog electronics are placed inside a stainless steel shielded room. The pumping lines of the cryostat are galvanically isolated from the gas handling system and the pumps. The cryostat is connected to the shielded room through the pumping lines.

To perform the timing measurement of the current, the trigger signals $V_{I,\rm TTL}$ and $V_{\rm TTL}$ are converted to digital optical pulses and passed via optical fibers out of the shielded room. There, both optical signals are converted back to TTL level electrical signals.

The repetition rate ν_I of the experiment is set, by a periodic TTL level square wave, which is converted to an optical signal and then passed via an optical fiber link into the shielded room, where it starts the current ramp. In each cycle of the measurement the bias current is increased at a fixed rate $\dot{I}$ until switching current I is reached.

The optically decoupled current and voltage trigger signals are then supplied to the start and stop inputs of a universal time interval counter to measure the time $\tau=t_{\rm start}-t_{\rm stop}$ between the trigger signals with a resolution of approximately 25 ps. Having calibrated the current ramp rate $\dot{I}$ the switching current can be calculated as $I=\dot{I}\tau$.

Similar time-based methods for measuring the junctions critical current at a constant current ramp rate[32,33] or the lifetime of the zero-voltage state of a junction at a constant applied bias current[18,40] have been implemented earlier by other groups.

The time interval counter[44] used in our setup allows ''on-the-fly'' generation of switching current histograms from the acquired data during the measurement. This feature is very useful for online monitoring of switching current histograms under changing experimental conditions, e.g., when doing spectroscopic measurements by applying microwave radiation to the sample or when searching for parasitic noise sources.

The temperature control system of the dilution refrigerator, which measures and controls the sample temperature in

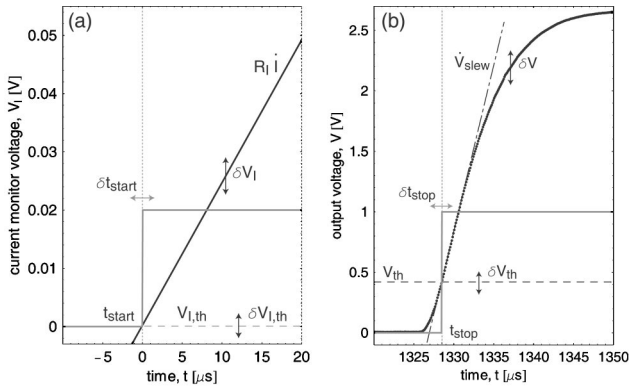

FIG. 4. (a) Current monitor voltage signal $V_I = R_I \dot{I}$ across the bias resistor (dark solid line). The zero crossing current trigger signal $V_{I,\mathrm{TTL}}$ starting at $t = t_{\mathrm{start}}$ (gray line), when trigger threshold $V_{I,\mathrm{th}}$ (dashed line) is reached, is superimposed. (b) Amplified voltage signal V across the junction (dark sold line). Voltage trigger threshold V_{th} is indicated (dashed line). The slew rate $\dot{V}$ at V_{th} is indicated (dash-dotted line). Voltage trigger signal V_{TTL} (gray line) with the edge rising at $t = t_{\mathrm{stop}}$ is superimposed on an arbitrary scale. Fluctuations of various parameters are indicated.

the range between 20 mK and 4.2 K, is installed in the shielded room. It is powered either by two lead batteries or via an isolation transformer. The electrical ground of the controller is anchored to the cryostat. The temperature controller is computer controlled via an optical fiber link.

C. Current resolution

First, we discuss the *instrumental* limit of the current resolution attainable with our setup imposed by the limited time resolution of the counter. Second, we consider the *practical* limits put on the current resolution due to the noise properties of the analog bias electronics.

Our timing method has a high *instrumental* current resolution of $\delta I_{\mathrm{inst}} = \dot{I} \cdot 25$ ps. In this scheme δI_{inst} is proportional to the current ramp rate but independent of the actual value of the measured current. For typical ramp rates between 0.1 and 1 A/s, used in the experiments presented here, *instrumental current resolution* between $\delta I_{\mathrm{inst}} = 2.5$ and 25 pA can be achieved. If we were to use a 16 bit analog to digital (A/D) converter for direct current measurements we would expect an instrumental resolution of $\delta I_{\mathrm{inst}} \approx \langle I \rangle / 2^{16} \approx \langle I \rangle 15 \times 10^{-6}$, which is proportional to the mean value $\langle I \rangle$ of the measured current. For typical values of $\langle I \rangle = 100$ μA used in the experiments presented here, we find $\delta I_{\mathrm{inst}} \approx 1.5$ nA, which is a factor of $10^2 - 10^3$ worse than the instrumental resolution that is reached using the timing technique.

In practice, the resolution of our switching current measurement is limited by the accuracy with which t_{start} and t_{stop} can be determined in the presence of electronics noise. As pointed out before, the instrumental rms resolution of the time interval counter $\delta t_{\mathrm{ins,rms}} \approx 25$ ps is high. The rms fluctuations in the measured times due to fluctuations in the bias electronics are typically much larger.

The rms fluctuations $\delta t_{\mathrm{start}}$ in t_{start} are governed by the voltage fluctuations of the input signals to the trigger circuits, i.e., the threshold voltage fluctuations and the voltage fluctuations of the current monitor signal, and the voltage noise of the trigger circuit itself; see Fig. 4(a). Those fluctuations are dominated by the rms input voltage noise $\delta V_{\mathrm{trig,rms}} \approx 20$ μV of the trigger circuit. The rms fluctuations $\delta V_{I,\mathrm{rms}}$ in the voltage measurement across the bias resistor and the rms fluctuations $\delta V_{I,\mathrm{th}}$ in the trigger threshold voltage are much smaller. Thus the fluctuations in the start time are given approximately by

$$\delta t_{\mathrm{start,rms}} \approx \frac{\delta V_{\mathrm{trig,rms}}}{G_I R_I \dot{I}}, \tag{12}$$

where $G_I R_I \dot{I}$ is the rate of change of the output voltage of the current monitor instrumentation amplifier operated at $G_I = 1$; see Fig. 4(a). For a bias resistor with $R_I = 10^4 \Omega$ and a ramp rate of $\dot{I} = 0.245$ A/s we find $\delta t_{\mathrm{start,rms}} \approx 8$ ns.

The rms variations $\delta t_{\mathrm{stop,rms}}$ in the time t_{stop} of the voltage trigger are dominated by the rms output voltage noise of the voltage amplifier $G_V \delta V_{\mathrm{rms}} \approx 6$ mV and depend on the slew rate $\dot{V}_{\mathrm{slew}}$ of the voltage signal at the amplifier output; see Fig. 4(b). The fluctuations of the voltage threshold level δV_{th} and the voltage noise of the comparator δV_{trig} are much smaller. The voltage slew rate $\dot{V}_{\mathrm{slew}}$ was determined by switching the junction from its zero-voltage state to the gap voltage and recording the output voltage of the amplifier versus time; see Fig. 4(b). $\dot{V}_{\mathrm{slew}}$, being effectively limited by the cutoff of the RC filters on the 1 K stage, was found to be $\dot{V}_{\mathrm{slew}} \approx 0.25$ V/μs.

Thus, the resulting rms variation in t_{stop} is given by

$$\delta t_{\mathrm{stop,rms}} = \frac{G^V \delta V_{\mathrm{rms}}}{\dot{V}_{\mathrm{slew}}}, \tag{13}$$

which for the experimentally determined parameters results in a value of $\delta t_{\mathrm{stop,rms}} \approx 22$ ns.

The total rms variation in the time measured $\tau = t_{\mathrm{stop}} - t_{\mathrm{start}}$ is then

$$\delta \tau_{\mathrm{rms}} = \sqrt{\delta t_{\mathrm{start,rms}}^2 + \delta t_{\mathrm{stop,rms}}^2}\ . \tag{14}$$

The rms noise in measured current I is accordingly given by $\delta I_{\mathrm{rms}} = \delta \tau_{\mathrm{rms}} \dot{I}$ and thus proportional to the current ramp rate $\dot{I}$. Here it is to be noted that the uncertainty in I due to the start trigger is independent of the current ramp rate $\dot{I}$, whereas the contribution due to the stop trigger increases linearly with $\dot{I}$. For a current ramp rate of $\dot{I} = 0.245$ A/s, typically used in our experiments, the resulting value for δI_{rms} is 5.6 nA. Thus for the typical mean switching current $\langle I \rangle \approx 325$ μA of the junction considered here, we expect relative fluctuations in $\langle I \rangle$ on the order of $\delta I_{\mathrm{rms}} / \langle I \rangle \approx 2 \times 10^{-5}$ due to the noise figures of the analog electronics.

IV. EXPERIMENTAL OBSERVATIONS

The experiments were performed using a high quality 5×5 μm^2 tunnel junction fabricated on an oxidized silicon wafer using a standard Nb/Al–AlO_x/Nb trilayer process.[45] The junction had a nominal critical current density of $j_c \approx 1.3$ kA/cm^2, a nominal capacitance of $C \approx 1.6$ pF and subgap resistance of $R > 500$ Ω below 1.0 K.

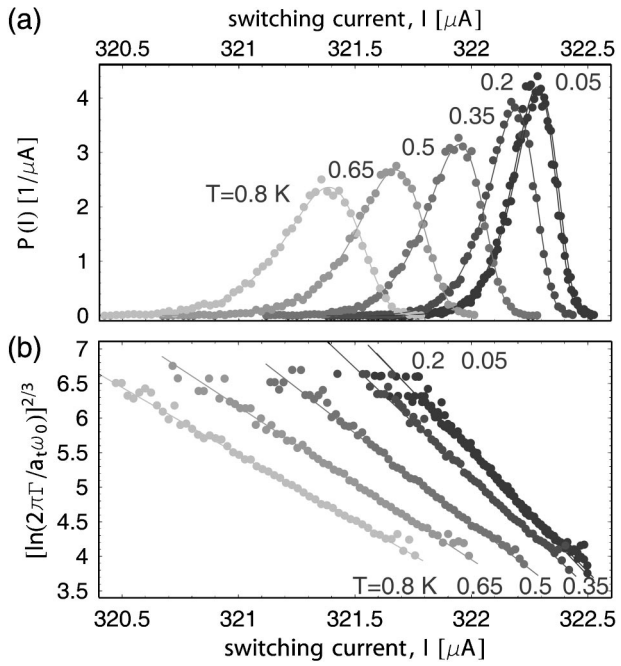

FIG. 5. (a) Switching current distributions $P(I)$ at bath temperatures between $T=50$ and 800 mK. (b) Normalized escape rate $\ln(2\pi\Gamma/a_t\omega_0)^{2/3}$ for the same bath temperatures. The symbols represent data, and the lines are fits.

The switching current distribution of the sample was measured at bath temperatures T between 20 and 800 mK in steps of 10 mK. The current was ramped up at a constant rate of $\dot{I}=0.245$ A/s with a repetition rate of $\nu_I=500$ Hz. Typically, 10^4 switching currents were recorded at each temperature. Histograms of the switching currents were calculated with bin widths ranging from 10 to 25 nA in order to determine the $P(I)$ distributions. In Fig. 5(a) the measured $P(I)$ distributions are plotted for a set of bath temperatures T. It is observed that the width of the $P(I)$ distributions decreases with the temperature and then saturates at low temperatures, as expected. Also, the mean switching current $\langle I\rangle$ is observed to decrease with the temperature and then saturate at low temperatures; also see upper inset of Fig. 7.

The standard deviation σ_I of $P(I)$ is plotted versus T in Fig. 6. In the temperature range between 800 and approximately 300 mK σ_I decreases with T, indicating temperature dependent thermal activation of the phase across the barrier. Below the characteristic temperature $T^\star\approx 300$ mK, σ_I saturates at approximately 105 nA, suggesting that escape of the phase is dominated by quantum tunneling through the barrier. In Sec. V, the $P(I)$ distributions in both the thermal and the quantum regime are analyzed quantitatively and compared with existing models.

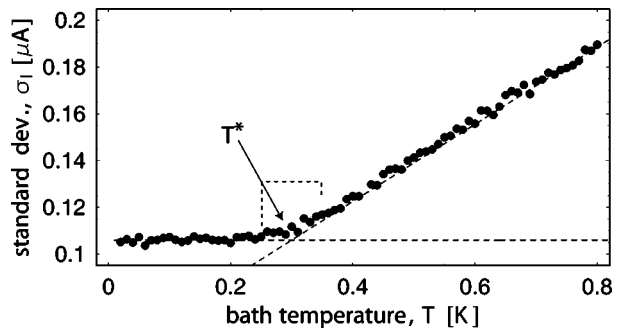

FIG. 6. Standard deviation σ_I of $P(I)$ distributions vs T. The characteristic crossover temperature $T^\star$ is indicated.

V. DATA ANALYSIS

A. Thermal activation

At temperatures $T>T^\star$ escape of the phase is dominated by thermal activation. At a fixed bias current the activation rate is given by Eq. (7). Using Eq. (11), the experimental escape rate $\Gamma(I)$ is determined from the $P(I)$ data and compared with the predictions of Eq. (7).

To perform this comparison we rewrite Eq. (7) using the known bias current dependence of the approximated barrier height, Eq. (6), and the small amplitude oscillation frequency, Eq. (5),

$$\left(\ln\frac{2\pi\Gamma(I)}{a_t\omega_0(I)}\right)^{2/3}=\left(\frac{E_J}{k_BT_{\rm esc}}\frac{4\sqrt{2}}{3}\right)^{2/3}\frac{1}{I_c}(I_c-I), \tag{15}$$

where we have introduced the effective escape temperature $T_{\rm esc}$.[15] The left-hand side of Eq. (15) is then calculated in a first iteration using the experimental data $\Gamma(I)$ and $a_t\omega_0(I)$ that is estimated approximating the initially unknown value of I_c by the maximum measured switching current $I_{\rm max}$ and using $C=1.61$ pF determined from independent microwave spectroscopy measurements[46] of the same sample. Because the right-hand side of Eq. (15) is a linear function of bias current I, both critical current I_c in the absence of fluctuations and effective temperature $T_{\rm esc}$ of the thermal activation process can be determined from a linear fit of the experimental data. The data are transformed according to the left-hand side of Eq. (15) and the linear fits are shown in Fig. 5(b). In the fitting procedure the data are weighted according to their statistical significance in the $P(I)$ distribution. Accordingly, we find

$$I_c=\frac{c_{\rm const}}{c_{\rm lin}}, \tag{16}$$

$$T_{\rm esc}=\frac{1}{k_B}\frac{\Phi_0}{2\pi}\frac{4\sqrt{2}}{3}\frac{1}{c_{\rm const}^{1/2}c_{\rm lin}}, \tag{17}$$

where $c_{\rm const}$ and $c_{\rm lin}$ are the two fitting parameters. The values of I_c and $T_{\rm esc}$ are then found with high accuracy by iteratively repeating the fitting procedure with the value of I_c found in the previous iteration.[10] This procedure converges rapidly due to the logarithmic dependence of the left-hand side of Eq. (15) on I_c.

We have extracted the effective escape temperature $T_{\rm esc}$ from the experimental data according to the procedure described above, taking into account the thermal prefactor a_t. According to simple transition state theory, the thermal prefactor is unity and the escape rate is determined only by the fraction of particles with energy larger than the barrier height. In the high as well as in the low damping regimes the prefactor deviates substantially from unity.[47]

The exact form of the prefactor is found from analysis of a classical Langevin equation for motion of the particle ac-

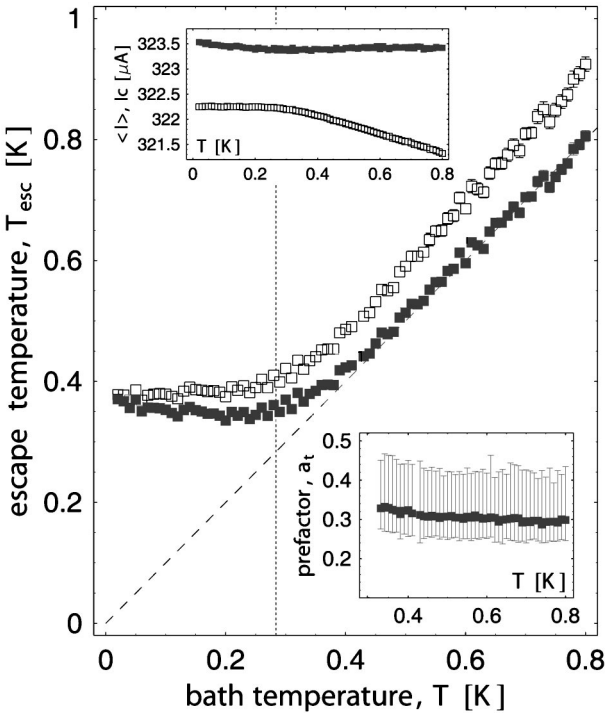

FIG. 7. Escape temperature T_{esc} vs bath temperature T extracted from experimental data for $a_t=1$ (open symbols) and a_t according to Eq. (18) (closed symbols). The statistical error in T_{esc} is less than the size of the symbol. The dashed line corresponds to $T=T_{esc}$. The dotted line indicates the calculated value of $T^{\star}$. The lower inset shows the value of a_t at the most probable switching current I_p vs T. The error bars indicate the value of a_t at the minimum I_{min} and maximum switching currents I_{max} within each $P(I)$ distribution. The upper inset shows the measured mean switching current $\langle I\rangle$ (open squares) and the critical current I_c (closed squares) from the fit vs T.

cording to Eq. (2) in the presence of fluctuations (see, e.g., Refs. 5 and 47). In the moderate to strong damping limit the value of a_t depends predominantly on the damping and the small oscillation frequency in the junction. In the very strong damping limit, the inertia of the particle can be neglected and its motion becomes diffusive.[7,8] In the low to extremely low damping regime, however, the distribution of particles in the well deviates from thermal equilibrium. The thermal escape across the barrier depletes the population within a range of k_BT to the top of the barrier. Therefore, a_t becomes dependent on the barrier height and on the temperature. Here we use an approximate analytical expression of the thermal prefactor, calculated in Ref. 48, for the extremely low to low damping regime, relevant for the experimental data presented here

$$a_t=\frac{4a_0}{(\sqrt{1+(a_0Qk_BT/1.8\,U_0)}+1)^2}, \tag{18}$$

where a_0 is a numerical constant close to unity and Q is the quality factor of the junction. An exact calculation of a_t that is valid in all damping regimes can be found in Ref. 5.

In the first step, T_{esc} was evaluated for $a_t=1$; see open symbols in Fig. 7. With this assumption, the escape temperatures extracted from the data deviates approximately 100 mK from the bath temperature for $T>T^{\star}$. The discrepancy between T_{esc} and T increases even more when the temperature is raised above 800 mK (data not shown). This deviation is too large to be due to inaccurate estimate of the junction capacitance or errors in calibration of the current measurement, thus, indicating the importance of the thermal prefactor.

In the second step, we used the thermal prefactor, Eq. (18), in our data analysis scheme with effective shunt resistance R as an adjustable parameter for determining the junction quality factor Q. We found good agreement between the escape temperature T_{esc} extracted and the bath temperature T for $R=240\Omega$, corresponding to a quality factor of biased junction of approximately $Q=95\pm5$; see closed symbols in Fig. 7. With the low damping prefactor, Eq. (18), the difference $|T_{esc}-T|$ is less than 15 mK for temperatures above 400 mK.

For a nominally identical sample, we have extracted the quality factor $Q\approx45\pm5$ from spectroscopic data[46] on the one-photon transition between the ground state and the first excited state of the phase below the crossover temperature $T^{\star}$. Considering the frequency dependence of the damping due to the electromagnetic environment and the accuracy with which the damping can be extracted from the thermal prefactor, the two independently determined values of Q are in reasonable agreement.

In the lower inset of Fig. 7, the thermal prefactor a_t evaluated at the most probable switching current I_p is plotted versus temperature for $T>T^{\star}$. The value of a_t is approximately 0.3 and is roughly independent of the bath temperature. This weak temperature dependence is attributed to the almost constant ratio of $k_BT/U_0(I_p)$ for the switching current data measured at different temperatures; see Eq. (18). At a fixed bath temperature, the variation in bias current within a single $P(I)$ distribution results in a noticeable variation of a_t. The value of a_t at the minimum and maximum switching currents, I_{min} and I_{max}, is indicated in the lower inset of Fig. 7 by error bars.

The critical current I_c extracted from the fits is plotted in the upper inset of Fig. 7 (closed symbols). For $T>T^{\star}$, I_c has a temperature independent value of 323.4 μA. For comparison, the temperature dependence of the mean switching current is also plotted (open symbols) in the upper inset of Fig. 7.

Thus, the experimental data at temperatures above $T^{\star}$ are explained well by the classical model of thermal activation of the phase over a potential barrier in the presence of extremely small damping.

However, in thermal activation theory, it is assumed that particle energies in the well are continuously distributed. For the sample considered here, quantization of the energy of the small amplitude oscillations of the phase may be relevant. In fact, we found direct evidence of energy level quantization of the phase in this and in similar samples using microwave spectroscopy.[46] At temperatures where thermal activation is observed in these experiments there are only a few levels in the well and the separation between levels is larger than k_BT. These facts indicate that the energy level structure may be relevant for the process of escape even at temperatures $T>T^{\star}$.

To analyze the effect of level quantization on escape of

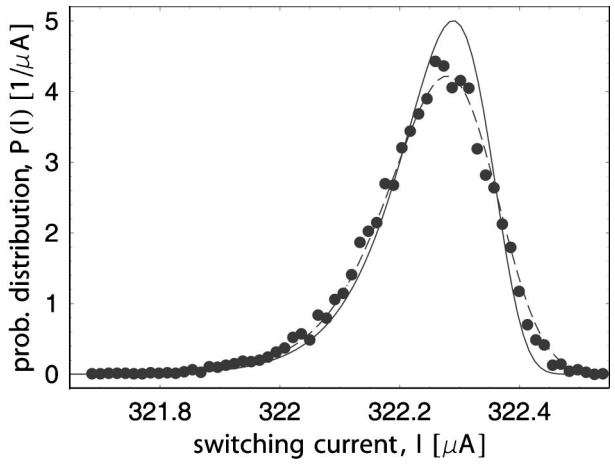

FIG. 8. Measured switching current distribution $P(I)$ at $T=20$ mK (closed symbols). The solid line is the predicted switching current distribution $P_q(I)$ in the quantum regime for $I_c=323.5$ μA and $C=1.61$ pF at $T=0$. The $P_q(I)$ distribution convoluted with a Gaussian distribution with the width of the experimental resolution is shown by the dashed line.

the phase at high temperatures we have made use of Larkin–Ovchinnikov theory.[49] Within the framework of this model, the escape of the phase is considered in terms of tunneling out of the well from individual energy levels. The overall escape rate $\Gamma_{\mathrm{LO}}(I)$ depends on the population of different levels, which is determined by the coupling to the thermal bath. To use this theory, we have calculated the energy level structure of the phase in the potential as dependent on bias current I. The matrix elements for transitions between individual levels were evaluated and the resulting escape rate was calculated by solving a master equation for the dynamics of the system. From the escape rate $\Gamma_{\mathrm{LO}}(I)$ we have calculated $P(I)$ distributions over a wide temperature range. The calculated $P(I)$ distributions at temperatures well below $T^{\star}$, when essentially only the ground state is populated, are in good agreement with the distributions calculated using the WKB approximation for tunneling from the ground state. At temperatures above $T^{\star}$, the $P(I)$ distributions calculated using Larkin–Ovchinnikov theory were consistent with our experimental data. More details on this analysis will be presented elsewhere.[50]

B. Quantum tunneling

At temperatures below the crossover temperature the escape of the phase from the potential well is dominated by quantum tunneling through the barrier. The crossover temperature,[36]

$$T^{\star}=\frac{\hbar\omega_0}{2\pi k_B}\left\{\left[1+\left(\frac{1}{2Q}\right)^2\right]^{1/2}-\frac{1}{2Q}\right\}, \tag{19}$$

for this sample evaluated at the most probable switching current I_p is approximately 280 mK, which is in good agreement with our experimental findings; see Fig. 6. Since the quality factor of this sample is $Q\approx 95$, the reduction of $T^{\star}$ in comparison to the ideal case of $Q=\infty$ is less than 1%. Accordingly, the reduction of the tunneling rate due to dissipation is small.

Furthermore, we have compared the measured $P(I)$ distributions for $T\ll T^{\star}$ to the predicted distributions calculated using the quantum tunneling rate, Eq. (8). As an example, the data for $T=20$ mK are shown in Fig. 8 by closed symbols. The quantum tunneling distribution $P_q(I)$ calculated for $I_c=323.5$ μA and $C=1.61$ pF is shown by the solid line. The critical current I_c was extracted from fits to the data in the thermal regime. The capacitance C was determined from independent spectroscopic measurements of the energy level structure of the same sample using the techniques described in Ref. 46. The most probable switching current of the calculated distribution is in good agreement with experimental data. However, the width of the measured distribution is slightly larger than that predicted. By calculating the convolution of the predicted quantum tunneling distribution $P_q(I)$ with a Gaussian current distribution that reflects the finite experimental resolution, we find good agreement between the experimental data and the theoretical prediction.

VI. DISCUSSION

The relative resolution of the switching current measurements demonstrated in this article is better than 3.5×10^{-4} at acquisition rates on the order of 10^3 events per second. The noise in the analog electronic circuits used in the setup limits the resolution to approximately 2×10^{-5}. The switching current distribution measurements presented here are comparable to the highest resolution measurements of this type performed so far. Recent developments in the field of quantum information processing have strongly increased the interest in research on the quantum properties of Josephson junction systems.[19,20,26–31] Using the measurement technique and setup described in this article the quantum mechanical properties of current biased Josephson junctions can be investigated with high accuracy.

ACKNOWLEDGMENTS

The authors would like to thank S. Lebeda, G. Logvenov, K. Urlichs, and M. Schuster for their technical help. They are indebted to M. H. Devoret, M. Fistul, and V. Kurin for useful discussions and to C. van der Wal and R. Schouten for their open minded collaboration. They acknowledge partial financial support of this project by the Deutsche Forschungsgemeinschaft (DFG) and by D-Wave Systems Inc.

[1] M. H. Devoret, D. Esteve, C. Urbina, J. Martinis, A. Cleland, and J. Clarke, *Quantum Tunneling in Condensed Media* (North-Holland, Amsterdam, 1992).
[2] W. C. Stewart, Appl. Phys. Lett. **12**, 277 (1968).
[3] D. E. McCumber, J. Appl. Phys. **39**, 3113 (1968).
[4] H. A. Kramers, Physica (Utrecht) **7**, 284 (1940).
[5] P. Hänggi, P. Talkner, and M. Borkovec, Rev. Mod. Phys. **62**, 251 (1990).
[6] A. O. Caldeira and A. J. Leggett, Phys. Rev. Lett. **46**, 211 (1981).
[7] J. M. Martinis and R. L. Kautz, Phys. Rev. Lett. **63**, 1507 (1989).
[8] D. Vion, M. Götz, P. Joyez, D. Esteve, and M. Devoret, Phys. Rev. Lett. **77**, 3435 (1996).
[9] T. A. Fulton and L. N. Dunkleberger, Phys. Rev. B **9**, 4760 (1974).
[10] M. Castellano *et al.*, J. Appl. Phys. **80**, 2922 (1996).
[11] B. Ruggiero, C. Granata, V. G. Palmieri, A. Esposito, M. Russo, and P. Silvestrini, Phys. Rev. B **57**, 134 (1998).

[12] J. M. Martinis, M. H. Devoret, and J. Clarke, Phys. Rev. B **35**, 4682 (1987).
[13] L. D. Jackel, J. P. Gordon, E. L. Hu, R. E. Howard, L. A. Fetter, D. M. Tennant, R. W. Epworth, and J. Kurkijärvi, Phys. Rev. Lett. **47**, 697 (1981).
[14] R. F. Voss and R. A. Webb, Phys. Rev. Lett. **47**, 265 (1981).
[15] M. H. Devoret, J. M. Martinis, and J. Clarke, Phys. Rev. Lett. **55**, 1908 (1985).
[16] P. Silvestrini, V. G. Palmieri, B. Ruggiero, and M. Russo, Phys. Rev. Lett. **79**, 3046 (1997).
[17] J. M. Martinis, M. H. Devoret, and J. Clarke, Phys. Rev. Lett. **55**, 1543 (1985).
[18] S. Han, Y. Yu, X. Chu, C.S., and Z. Wang, Science **283**, 1457 (2001).
[19] Y. Yu, S. Han, X. Chu, S.-I. Chu, and Y. Wang, Science **296**, 889 (2002).
[20] J. M. Martinis, S. Nam, J. Aumentado, and C. Urbina, Phys. Rev. Lett. **89**, 117901 (2002).
[21] M. F. Bocko, A. M. Herr, and M. J. Feldman, IEEE Trans. Appl. Supercond. **7**, 3638 (1997).
[22] Y. Makhlin, G. Schön, and A. Shnirman, Nature (London) **398**, 305 (1999).
[23] J. E. Mooij, T. P. Orlando, L. Levitov, L. Tian, C. H. van der Wal, and S. Lloyd, Science **285**, 1036 (1999).
[24] L. B. Ioffe, V. B. Geshkenbein, M. V. Feigel'man, A. L. Fauchere, and G. Blatter, Nature (London) **398**, 679 (1999).
[25] Y. Makhlin, G. Schön, and A. Shnirman, Rev. Mod. Phys. **73**, 357 (2001).
[26] Y. Nakamura, Y. A. Pashkin, and J. S. Tsai, Nature (London) **398**, 786 (1999).
[27] J. R. Friedman, V. Patel, W. Chen, S. K. Tolpygo, and J. E. Lukens, Nature (London) **406**, 43 (2000).
[28] C. H. van der Wal, A. C. J. ter Haar, F. K. Wilhelm, R. N. Schouten, C. J. P. M. Harmans, T. P. Orlando, S. Lloyd, and J. E. Mooij, Science **290**, 773 (2000).
[29] D. Vion, A. Aassime, A. Cottet, P. Joyez, H. Pothier, C. Urbina, D. Esteve, and M. H. Devoret, Science **296**, 886 (2002).
[30] Y. A. Pashkin, T. Yamamoto, O. Astafiev, Y. Nakamura, and J. S. Tsai, Nature (London) **421**, 823 (2003).
[31] I. Chiorescu, Y. Nakamura, C. J. P. M. Harmans, and J. E. Mooij, Science **299**, 1869 (2003).
[32] P. Silvestrini, S. Pagano, R. Cristiano, O. Liengme, and K. E. Gray, Phys. Rev. Lett. **60**, 844 (1988).
[33] P. Silvestrini, O. Liengme, and K. E. Gray, Phys. Rev. B **37**, 1525 (1988).
[34] E. Turlot, D. Esteve, C. Urbina, J. M. Martinis, M. H. Devoret, S. Linkwitz, and H. Grabert, Phys. Rev. Lett. **62**, 1788 (1989).
[35] S. Washburn, R. A. Webb, R. F. Voss, and S. M. Faris, Phys. Rev. Lett. **54**, 2712 (1984).
[36] H. Grabert and U. Weiss, Phys. Rev. Lett. **53**, 1787 (1984).
[37] A. O. Caldeira and A. J. Leggett, Ann. Phys. (NY) **149**, 374 (1983).
[38] A. J. Leggett, *Percolation, Localization, and Superconductivity* (Plenum, New York, 1984).
[39] B. Ruggiero, M. G. Castellano, G. Torrioli, C. Cosmelli, F. Chiarello, and V. G. Palmieri, Phys. Rev. B **59**, 177 (1999).
[40] M. H. Devoret, J. M. Martinis, D. Esteve, and J. Clarke, Phys. Rev. Lett. **53**, 1260 (1984).
[41] Thermocoax GmbH, Hamburg, Germany.
[42] A. B. Zorin, Rev. Sci. Instrum. **66**, 4296 (1995).
[43] D. Vion, P. F. Orfila, P. Joyez, D. Esteve, and M. H. Devoret, J. Appl. Phys. **77**, 2519 (1995).
[44] Stanford Research Systems, Sunnyvale, CA 94089, model SR 620 Universal Time Interval Counter.
[45] Hypres Inc., Elmsford, NY 10523.
[46] A. Wallraff, T. Duty, A. Lukashenko, C. Coqui, and A. V. Ustinov, Phys. Rev. Lett. **90**, 037003 (2003).
[47] U. Weiss, *Quantum Dissipative Systems*, 2nd ed. (World Scientific, Singapore, 1999).
[48] M. Büttiker, E. P. Harris, and R. Landauer, Phys. Rev. B **28**, 1268 (1983).
[49] A. I. Larkin and Y. N. Ovchinnikov, Sov. Phys. JETP **64**, 185 (1986).
[50] T. Duty and A. Wallraff (unpublished).